ChemComm

COMMUNICATION

Soft-templating synthesis of mesoporous magnetic $CuFe_2O_4$ thin films with ordered 3D honeycomb structure and partially inverted nanocrystalline spinel domains†

Christian Reitz,[a] Christian Suchomski,[a] Jan Haetge,[a] Thomas Leichtweiss,[a] Zvonko Jagličić,[b] Igor Djerdj[c] and Torsten Brezesinski*[a]

Combining sol–gel chemistry with polymer templating strategies enables production of $CuFe_2O_4$ thin films with both an ordered cubic network of 17 nm diameter pores and tunable spinel domain sizes. These nanocrystalline materials contain only minor structural defects with $\lambda = 0.85 \pm 0.02$ and exhibit multiple functionalities, including superparamagnetic behavior ($T_B \approx 310$ K) and redox- and photoactivity.

Transition metal ferrites with the general formula MFe_2O_4 (M = Cu, Co, Ni, *etc.*) constitute an important class of spinel oxides that exhibit a broad range of interesting physical properties. Therefore such materials are used in applications, such as magnetic recording, high-frequency devices, and so forth.

In recent years, it has been shown that MFe_2O_4 ferrites can adopt normal, inverse, and partially inverted or even mixed spinel structures.[1] As a result, the magnetic, optical, and electronic properties can be tailored through the variation of cations on the tetrahedral and octahedral coordination sites. However, it is also known that physical properties can be tailored by controlling both the grain size and the material morphology itself. Many materials have therefore seen benefits from structuring at the nanoscale in that they were able to outperform their bulk counterparts.

Among the existing transition metal ferrites, copper ferrite ($CuFe_2O_4$) plays an important role. As opposed to most MFe_2O_4 ferrites that crystallize in a cubic $Fd\bar{3}m$ spinel structure, $CuFe_2O_4$ is characterized by a tetragonal $I4_1/amd$ structure (Jahn–Teller effect) at room temperature.[2] In the present work, we specifically focus on mesoporous $CuFe_2O_4$ spinel thin films, materials that as we show here can be readily produced with both a 3D honeycomb structure and tunable nanocrystalline domain sizes. We use these spinel materials as model systems

both to study the cation distribution, relative to bulk versions of $CuFe_2O_4$, and to examine the magnetic properties.

In the past decade, it has been shown that polymer templating strategies are efficient routes to produce nanocrystalline metal oxides with mesoporous morphologies.[3] The formation of these materials relies on the solution phase coassembly of inorganic sol–gel precursors with an organic structure-directing agent, in particular amphiphilic polymers. The corresponding thin films can be achieved by the same coassembly methods but using an evaporation-induced self-assembly (EISA) process.[4]

The mesoporous $CuFe_2O_4$ thin films were produced using an EISA process. In this work, we incorporated a KLE-type diblock copolymer (here $H[(CH_2CH_2)_{0.67}(CH_2CHCH_2CH_3)_{0.33}]_{89}$–$(OCH_2CH_2)_{79}OH)$) as the structure-directing agent and hydrated copper and ferric nitrate salts as the precursors (see the Experimental procedure in ESI†).[5]

To probe the nanoscale structure, both transmission (TEM) and scanning electron microscopy (SEM) were used. Fig. 1 shows TEM and SEM data of KLE-templated $CuFe_2O_4$ spinel thin films heated to 650 °C. The top view SEM images in panels (a) and (b) reveal a cubic network of interconnected pores averaging 17 nm in diameter; the total porosity is ∼30% (see also Fig. S1 and S2 in ESI†). It is evident from these data that the presence of larger structural defects can be ruled out after conversion of the amorphous material to nanocrystalline spinel. It can also be seen that the pore walls are up to 17 nm thick, which helps explain why the nanoscale structure is retained after crystallization. From the TEM images in panels (c) and (d), we are able to establish that the honeycomb pore network observed at the hexagonal top surface persists throughout the films. TEM further shows that the pore walls consist of particulate nanodomains. The average size of these domains is consistent with the pore wall thickness determined from SEM. The inset in panel (c) shows a selected-area electron diffraction (SAED) pattern of the same film used for TEM imaging. The presence of diffuse Debye–Scherrer rings is typical of a nanocrystalline material with randomly oriented domains. Calculated lattice spacings are in agreement with tetragonal $CuFe_2O_4$.[5] The crystalline nature is also confirmed by high-resolution TEM (HRTEM), as can be seen in the inset in panel (d). Overall, both SEM and TEM indicate that the spinel materials are well-defined at the nanoscale and the microscale.

[a] *Institute of Physical Chemistry, Justus-Liebig-University Giessen, Heinrich-Buff Ring 58, 35392 Giessen, Germany. E-mail: torsten.brezesinski@phys.chemie.uni-giessen.de*

[b] *Institute of Mathematics, Physics and Mechanics & Faculty of Civil and Geodetic Engineering, University of Ljubljana, Jadranska 19, 1000 Ljubljana, Slovenia*

[c] *Ruđer Bošković Institute, Bijenička 54, 10000 Zagreb, Croatia*

† Electronic supplementary information (ESI) available: Experimental procedure, SEM–TEM images, TGA-MS data, Kr-physisorption data, UV-vis data, photobleaching data, XPS data, galvanostatic charge–discharge curves. See DOI: 10.1039/c2cc31006f
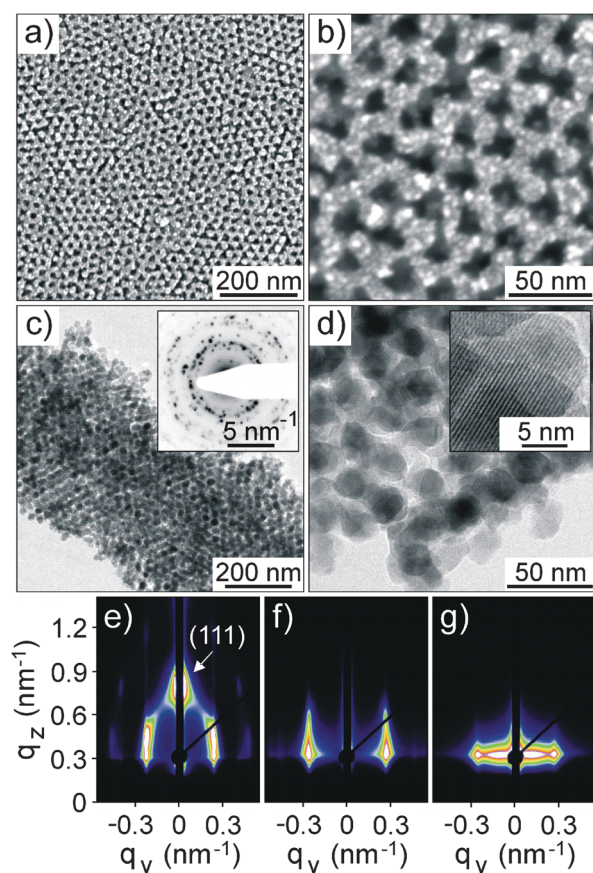
Fig. 1 (a–d) Morphology and nanoscale structure of KLE-templated $CuFe_2O_4$ spinel thin films heated to 650 °C. (a, b) Top view SEM images. (c, d) TEM images. The inset in panel (c) shows a SAED pattern. The inset in panel (d) displays a HRTEM image showing the (101) lattice planes of tetragonal $CuFe_2O_4$. (e–g) Synchrotron-based GISAXS at an angle of incidence $\beta = 0.2°$ on thin films heated at 300 °C for 12 h (e), and 600 °C (f) and 700 °C (g) for 10 s, respectively.

More quantitative information on the pore structure of the KLE-templated thin films was obtained by grazing incidence small-angle X-ray scattering (GISAXS, see Fig. 1e–g). Amorphous samples produce patterns with distinct maxima that can be indexed to a face-centered-cubic close-packed structure with (111) orientation. The elliptical shape of the GISAXS pattern in panel (e) further indicates a large unidirectional lattice contraction. This result is not surprising, however, because the $CuFe_2O_4$ thin films are both solution processed *via* sol–gel methods and bound to the substrate.

A decrease in film volume of $\sim 70\%$ is determined for samples heated at 300 °C for 12 h. Higher annealing temperatures do not lead to further contraction because the various iron and copper hydroxy- and oxynitrate species that are formed during thermal annealing are fully decomposed at 300 °C (see Fig. S3 in ESI†). Upon heating the films to 600 °C to crystallize the framework, a loss of out-of-plane scattering is observed. This loss can be attributed both to the small number of repeat units in this direction and to the process of crystallizing the inorganic wall structure itself. GISAXS data recorded at 700 °C indicate the appearance of new, diffuse in-plane maxima at lower **q**-values. These maxima arise because of restructuring of the honeycomb pore network due to crystalline domain growth (see Fig. 2a).
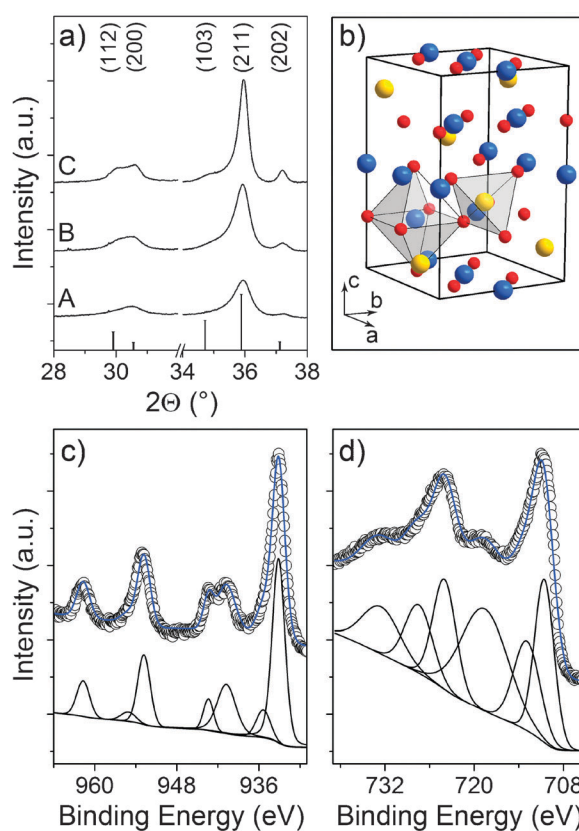

Fig. 2 (a) WAXD patterns of KLE-templated $CuFe_2O_4$ spinel thin films heated to 600 °C (A), 650 °C (B), and 700 °C (C). The line pattern shows JCPDS card no. 34-0425. (b) Scheme of the tetragonal unit cell with purely inverse spinel structure. Iron atoms occupying the tetrahedral 4(a) sites are shown in yellow, copper and iron atoms on octahedral 8(d) sites in blue, and oxygen atoms on 16(h) sites in red. The different coordination spheres are indicated by polyhedra. Note that one additional oxygen atom was added to draw the octahedron. (c, d) XPS spectra of the Cu2p and Fe2p core levels. Black lines are fits to the data assuming Shirley background. Blue lines correspond to the sum of the peak fits.

Apart from the nanoscale structure, we also analyzed the optical properties of the KLE-templated thin films. UV-vis data (see Fig. S4 in ESI†) indicate an indirect band gap at (1.40 ± 0.05) eV, which is in fair agreement with *ab initio* DFT calculations of 1.20 eV.[6] The slight blue-shift is reasonable since the spinel domains in the walls are nanocrystalline and partially inverted. Because of the small band gap energy and high specific surface area/porosity, the $CuFe_2O_4$ materials also show promise as novel visible-light-responsive photocatalysts for the degradation of organic pollutants, in particular as Fenton-like catalysts with enhanced activity and stability (see Fig. S5 in ESI†).

To study the crystallization behavior of the sol–gel derived $CuFe_2O_4$ samples, a series of wide-angle X-ray diffraction (WAXD) measurements was carried out. The WAXD patterns in Fig. 2a show the films to be composed of purely tetragonal $CuFe_2O_4$, as corroborated by JCPDS reference card no. 34-0425. The crystallization begins at approximately 580 °C. The average crystalline domain sizes start at 10 nm and can be tuned up to 16 nm at 650 °C. The latter value is in agreement with the size of the spinel domains determined from TEM. WAXD data at 700 °C provide a crystallite size of 22 nm, and thus give an explanation for the loss of nanoscale periodicity both in the

off- and in-plane direction; the spinel domains are larger than the wall thickness and this mismatch leads to restructuring mentioned above.

Bulk versions of tetragonal $CuFe_2O_4$ are known to adopt a spinel structure with virtually complete inversion (see Fig. 2b). In this structure, Cu^{2+} ions occupy mainly the octahedral sites, while Fe^{3+} ions are located both on the tetrahedral and on the octahedral sites in about equal amounts. The cation distribution is typically analyzed in terms of the inversion parameter, λ. There are two ordered configurations with $\lambda = 0$ (normal) and $\lambda = 1$ (inverse). Many ferrites, however, exhibit a partially inverted spinel structure, which is largely dependent on the synthesis method used.

In the ensuing sections, we specifically focus on $CuFe_2O_4$ thin films heated to 650 °C. To determine the inversion parameter, X-ray photoelectron spectroscopy (XPS) measurements were carried out. Fig. 2c and d show XPS scans of the Cu2p and Fe2p core level regions (see also Fig. S6 in ESI†). The slight asymmetry of the Cu2p lines towards higher binding energies indicates that the spinel structure is partially inverted. The main peaks at binding energies of (952.81 ± 0.05) eV and (933.13 ± 0.05) eV for the $Cu2p_{1/2}$ and $Cu2p_{3/2}$ lines, respectively, are assigned to Cu^{2+} on octahedral sites, while the minor ones at (955.08 ± 0.05) eV and (935.36 ± 0.05) eV can be assigned to Cu^{2+} on tetrahedral coordination sites. Elemental analysis carried out by comparing the different peak areas provides an inversion parameter $\lambda = 0.85 \pm 0.02$, corresponding to $[Cu_{0.15}Fe_{0.85}]_{tet}[Cu_{0.85}Fe_{1.15}]_{oct}O_4$. Lastly, we note that the appearance of strong satellite peaks is characteristic of copper being in the oxidation state $+2$. We also examined the Fe2p core level region in detail. First, the Fe2p spectrum indicates only the Fe^{3+} oxidation state. Second, both lines can be fit to two peaks (see also Table S1 in ESI†). More importantly, however, the same inversion parameter is found, which confirms the accuracy of the calculated value for λ.

The magnetic properties were analyzed using a SQUID magnetometer. Fig. 3a–d show both typical zero field cooled (ZFC) and field cooled (FC) curves and M–H plots for different applied field directions. The data in panel (a) reveal irreversibility between the ZFC and FC curves. For in-plane experiments, the ZFC magnetization exhibits a broad maximum centered at approximately 310 K. This maximum can be assigned to the blocking temperature, T_B, of the $CuFe_2O_4$ material. The FC magnetization, by contrast, slightly increases with decreasing temperature. Off-plane experiments reveal a similar trend; however, the overall magnetization is lower and T_B is shifted to temperatures outside the range experimentally measurable by our equipment. The reason for this might be related to strain anisotropy resulting from the unidirectional film contraction.[7] Panels (b–d) show M–H plots recorded at 5 K and 300 K. First, it is evident that the magnetization is not saturated at an applied field of 50 kOe at either of the two temperatures. On the basis of the calculated inversion parameter, the $CuFe_2O_4$ thin films are expected to have a saturation magnetization M_S of ~ 51 emu g^{-1} (~ 2.2 μ_B per formula unit), which is, in fact, larger than the ~ 40 emu g^{-1} measured value. Second, it can be seen that orientation has no effect on the coercivity, H_C, but the magnetization values are slightly different with $M_{in-plane} > M_{off-plane}$. This result
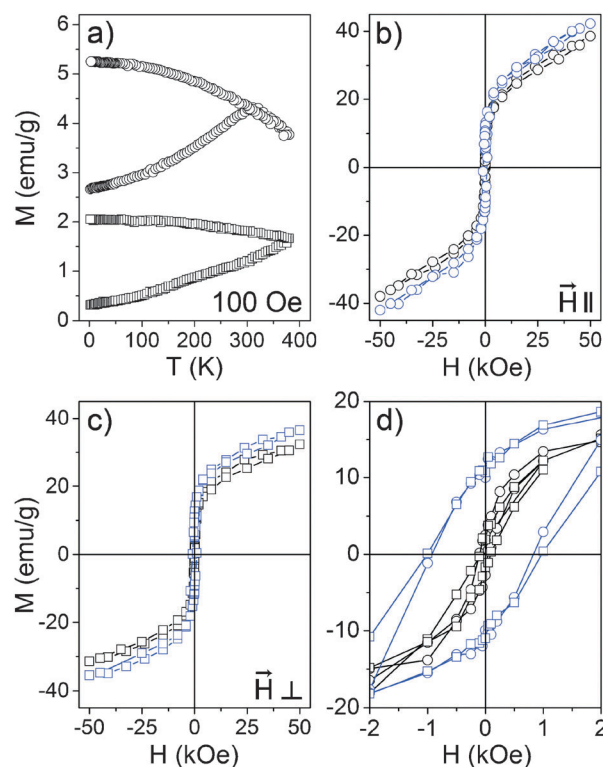

Fig. 3 Magnetic properties of KLE-templated $CuFe_2O_4$ spinel thin films heated to 650 °C. (a) ZFC and FC curves for samples oriented both with the plane of the substrate perpendicular (squares) and parallel (circles) to the external magnetic field. (b, c) Hysteresis experiments at 5 K (blue) and 300 K (black). (d) Hysteresis loops within the field range of ± 2 kOe.

indicates that the magnetic easy axis lies parallel to the substrate due to shape anisotropy. Third, the M–H plots show that the mesoporous spinel materials exhibit ferrimagnetic behavior with moderate coercivity of ~ 1 kOe at 5 K. At 300 K, both the coercivity and the remanence are negligible (but not zero), indicating superparamagnetic behavior above, and close to, T_B.

In summary, we have shown that $CuFe_2O_4$ can be templated to produce high quality mesoporous magnetic thin films with partially inverted spinel domains. These materials exhibit multiple functionalities, including redox- and photoactivity (see Fig. S5 and S7 in ESI†), and thus could pave the way for innovative device design.

Notes and references

1 H. S. C. Oneill and A. Navrotsky, *Am. Mineral.*, 1983, **68**, 181.
2 J. D. Dunitz and L. E. Orgel, *J. Phys. Chem. Solids*, 1957, **3**, 20.
3 C. Sanchez, B. Boissiere, D. Grosso, C. Laberty and L. Nicole, *Chem. Mater.*, 2008, **20**, 682.
4 C. J. Brinker, Y. F. Lu, A. Sellinger and H. Y. Fan, *Adv. Mater.*, 1999, **11**, 579.
5 J. Haetge, C. Suchomski and T. Brezesinski, *Inorg. Chem.*, 2010, **49**, 11619.
6 M. Feng, A. Yang, X. Zuo, C. Vittoria and V. G. Harris, *J. Appl. Phys.*, 2010, **107**, 09A521.
7 T. E. Quickel, V. H. Le, T. Brezesinski and S. H. Tolbert, *Nano Lett.*, 2010, **10**, 2982.